Nonlinear Dyn (2021) 106:3637–3646
https://doi.org/10.1007/s11071-021-06955-6

ORIGINAL PAPER

Effect of excited state lasing on the chaotic dynamics of spin QD-VCSELs

Panagiotis Georgiou · Christos Tselios · Georgia Mourkioti · Charalampos Skokos · Dimitris Alexandropoulos

Received: 16 June 2021 / Accepted: 29 September 2021 / Published online: 18 October 2021

Abstract We investigate numerically the chaotic dynamics of optically pumped quantum-dot (QD) spin vertically coupled surface emitting lasers (VCSELs) accounting for both ground state (GS) and excited state (ES) energy levels through the elaboration of the spin-flip model (SFM). The intensity dynamics associated with ES and GS transitions are studied by means of the largest Lyapunov exponent (LLE) and stability maps in terms of operational parameters (pump ellipticity and pump intensity), as well as material parameters (ES–GS intraband relaxation rate, spin relaxation rate and birefringence), are produced. It is established that although both ES and GS dynamics exhibit the same kind of nonlinear dynamics for a given set of control parameters, the ES and GS dynamics are weakly uncorrelated. This can be the basis for the realization of various functionalities including reservoir computing.

Keywords Semiconductor lasers · Quantum-dot spin VCSELs · Chaos · Nonlinear dynamics · Largest Lyapunov exponent · Neuromorphic photonics · Reservoir computing

P. Georgiou (✉) · C. Tselios · G. Mourkioti · D. Alexandropoulos
Department of Materials Science, University of Patras, Rion, 26504 Achaia, Greece
e-mail: panagiotis.georgiou@upnet.gr

D. Alexandropoulos
e-mail: dalexa@upatras.gr

C. Skokos
Nonlinear Dynamics and Chaos group, Department of Mathematics and Applied Mathematics, University of Cape Town, Rondebosch, Cape Town 7701, South Africa

1 Introduction

The interest in polarization dynamics in spin-vertical cavity surface emitting lasers (VCSELs) has increased in recent years [1–5]. In these devices, it is possible to control the output optical polarization by injecting spin-polarized electrons. Spin-polarized VCSELs can exhibit a plethora of nonlinear phenomena, ranging from oscillatory operation (single, period doubling, etc.) all the way to chaos, without the requirement for an external feedback perturbation or optical injection [6–8]. It is the spin property of the injected carriers and the coupling with the circularly polarized optical field that gives rise to nonlinear phenomena.

Recently, ultrafast polarization dynamics [9] and in particular polarization frequencies in spin VCSELs of 200 GHz or higher [10] have paved the way for energy efficient ultrafast optical communication. Additionally, attention in the field is fueled by the potential of VCSELs for neuromorphic photonics [11,12], as well as secure communications [5,13]. Retaining the spin polarization during the injection process it is indeed a demanding yet addressable task. For this either spin-injecting electrical contacts [14] or optical pumping [15–17] have been used.

The operation of spin-polarized VCSELs can be theoretically studied in the context of the spin-flip model

(SFM) [18] which describes in a simple and intuitive manner complex processes yielding the set of rate equations (REs) that are not computationally demanding. In this context we end up with four level coupled rate equations for quantum wells (QWs) or six for quantum dots (QDs) [17,19]. According to SFM, in the absence of an external magnetic field, the oscillatory operation of the spin-polarized VCSELs is the outcome of the competition between spin relaxation processes (γ_s), dichroism (γ_a) and birefringence (γ_p) [19].

The spin-polarized VCSEL literature is monopolized with theoretical and experimental works on QW spin VCSELs (see, e.g., [20–23]), while there are a few accounts of QD spin-polarized VCSELs [24,25]. QD spin VCSELs provide additional degrees of freedom for controlling polarization dynamics and these include the interband relaxation rates [wetting layer (WL) to ground state (GS)] [6], modified gain parameter (h) and variable linewidth enhancement factor (α) [25,26]. In [27], the SFM model was modified for the case of QD spin VCSELs and the spin dynamics were studied initially by means of the largest Lyapunov exponent (LLE) and elaborated in [6] with bifurcation theory (BT). More specifically, in [6] a detailed study of the dynamics of spin-polarized QD-VCSELs is presented where the different dynamical regions and key bifurcations are mapped using the modified SFM model. The findings of [6] have verified the role of key design parameters specific to the QDs, i.e., the capture rate from WL to QD ground state (γ_0), the gain coefficient (h) and the α-factor in tuning the dynamical characteristics. The majority of published works to date on QD spin lasers account only for the effects of WL and GS energy levels. [7,28,29]

Noticeably, a study of the effects of ES lasing is missing from the literature. Hence, a study of ES lasing on the polarization characteristics is now due for progressing present understanding on key parameter effects (material and operational) and control of spin-polarized VCSELs. This formulates the scope of the present work; here we modify further the SFM QD spin VCSEL model to include the ES and use this to study numerically the dynamics of both fields associated with GS and ES transitions. The rest of the paper is organized as follows: in Sect. 2, we present the modification of the SFM model to account for ES and the normalization of the SFM rate equations is analyzed. The model is numerically studied in Sect. 3 and the relevant results are discussed. In Sect. 4, we discuss potential applications of the proposed structure. We summarize the main findings of our work in Sect. 5.

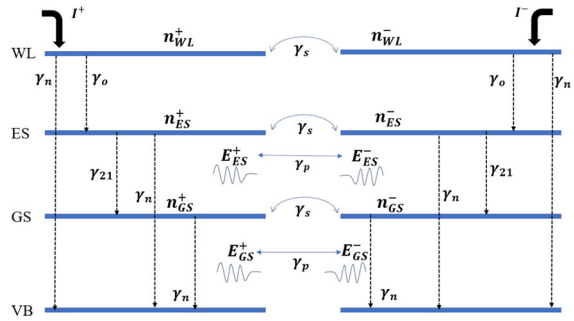

Fig. 1 Schematic representation of the energy levels (WL, ES, GS, VB) and transitions of carriers in the 8-level system used for the SFM in the QD spin-VCSEL

2 SFM model accounting for ES

2.1 Modification of the SFM model

The starting point of our analysis is the QD spin-VCSEL model developed in [6]. The model of [6] accounts only for WL and GS energy levels.

We introduce the ES level in a similar manner as commonly done for conventional (i.e., non spin) QD systems [30], but here the carriers and fields related to WL, ES and GS are spin resolved thus producing a 8-level rate equation system. In the following, the upward carrier transitions are neglected [27]. The spin resolved energy diagram of QD system along with the relevant transitions used in this study is shown in Fig. 1. The ES is fourfold degenerate and the GS is twofold degenerate [30]. The spin-polarized carriers, spin-up ($-$) and spin-down ($+$), are generated in the WL via optical pumping. The capture rate to the ES level is γ_0. The spin-polarized carriers at the ES relax at the spin-up(down) GS level with an intra-dot relaxation rate γ_{21}. Intra-dot spin-relaxation process can occur from spin-up(down) ES to spin-down(up) ES as well as from spin-up(down) GS to spin-down(up) GS at a rate γ_s. Lasing occurs via transitions from the ES or GS, to the valence band (VB) emitting right (E^+_{ES}, E^+_{GS}) and left (E^-_{ES}, E^-_{GS}) circularly polarized electric fields at two distinct wavelengths. The right and left circularly polarized fields are coupled via birefringence rate γ_p and dichroism γ_a. The above physical process is described by a set of REs, consisting of six equations for the dynamics

of carriers ($f^{\pm}_{WL}$, $f^{\pm}_{ES}$, $f^{\pm}_{GS}$) and four equations for the dynamics of the electric field amplitudes ($E^{\pm}_{GS}$, $E^{\pm}_{ES}$). The complete set of REs describing the modified SFM model reads as:

$$\frac{df^{\pm}_{WL}}{dt} = \frac{I^{\pm}}{eN_{WL}} - \gamma_0 f^{\pm}_{WL}(1 - f^{\pm}_{ES}) - \gamma_n f^{\pm}_{WL} \mp \gamma_s (f^{+}_{WL} - f^{-}_{WL}) \quad (1)$$

$$\frac{df^{\pm}_{ES}}{dt} = \frac{1}{4}\frac{N_{WL}}{N_{QD}}\gamma_0 f^{\pm}_{WL}(1 - f^{\pm}_{ES}) - \gamma_n f^{\pm}_{ES} - \gamma_{21} f^{\pm}_{ES}(1 - f^{\pm}_{GS}) - v_g \Gamma 2a(2f^{\pm}_{ES} - 1)|E^{\pm}_{ES}|^2 \mp \gamma_s (f^{+}_{ES} - f^{-}_{ES}) \quad (2)$$

$$\frac{df^{\pm}_{GS}}{dt} = 2\gamma_{21} f^{\pm}_{ES}(1 - f^{\pm}_{GS}) - \gamma_n f^{\pm}_{GS} - v_g \Gamma a(f^{\pm}_{GS} - 1)|E^{\pm}_{GS}|^2 \mp \gamma_s (f^{+}_{GS} - f^{-}_{GS}) \quad (3)$$

$$\frac{dE^{\pm}_{GS}}{dt} = k[h_1(2f^{\pm}_{GS} - 1) - 1](1 + i\alpha)E^{\pm}_{GS} - (\gamma_a + i\gamma p)E^{\mp}_{GS} \quad (4)$$

$$\frac{dE^{\pm}_{ES}}{dt} = k[h_2(2f^{\pm}_{ES} - 1) - 1](1 + i\alpha)E^{\pm}_{ES} - (\gamma_a + i\gamma p)E^{\mp}_{ES}. \quad (5)$$

Here, $f^{\pm}_{ES}$, $f^{\pm}_{GS}$ describe, respectively, the occupation probability of ES and GS energy levels. The amplitude of the electric field is, respectively, denoted by $E^{\pm}_{ES}$, $E^{\pm}_{GS}$ for transitions involving ES and GS levels. The dichroism rate is γ_a, e is the electron charge, N_{WL} denotes the density of states in the WL and N_{QD} the density of dots per volume, a is the differential gain and α is the linewidth enhancement factor. The cavity loss rate k is defined as $k = (2\tau_p)^{-1}$, where τ_p is the photon lifetime. The normalized gain coefficient h_1 for GS transitions is defined by $h_1 = v_g \Gamma a N_{QD} \tau_p$, where v_g is the group velocity and Γ is the optical confinement factor. For ES transitions, the gain coefficient is $h_2 = 2h_1$ [31].

2.2 Normalization of the modified SFM

For the normalization of the system of REs, we introduce a change in variables as follows:

$$n^{\pm}_{ES} = h_2(2f^{\pm}_{ES} - 1) \quad (6)$$

$$n^{\pm}_{GS} = h_1(2f^{\pm}_{GS} - 1) \quad (7)$$

$$n^{\pm}_{WL} = h_2\frac{N_{WL}}{N_{QD}} f^{\pm}_{WL} \quad (8)$$

$$E^{\pm}_{s,ES} = E^{\pm}_{ES}\sqrt{\frac{v_g \Gamma 2a}{\gamma_n}} \quad (9)$$

$$E^{\pm}_{s,GS} = E^{\pm}_{GS}\sqrt{\frac{v_g \Gamma a}{\gamma_n}} \quad (10)$$

$$\eta^{\pm} = \frac{I^{\pm} - I^{\pm}_{GS,th}}{I^{\pm}_{ES,th} - I^{\pm}_{GS,th}} \quad (11)$$

where $\eta^{\pm}$ is the normalized pumping term. The carrier injection at GS and ES threshold is, respectively, denoted by $I^{\pm}_{GS,th}$ and $I^{\pm}_{ES,th}$. $I^{\pm}$ is the value of the injected spin-polarized current density. ES lasing occurs for $\eta^{\pm} > 1$, i.e., for $I > I^{\pm}_{ES,th}$. The normalized polarized field from the ES is $E^{\pm}_{s,ES}$ and from the GS is $E^{\pm}_{s,ES}$. The normalized carrier populations occupying energy levels WL, ES and GS are denoted by $n^{\pm}_{WL}$, $n^{\pm}_{ES}$, $n^{\pm}_{GS}$, respectively. The normalization process follows that of [27] except for the definition of the normalized pumping term $\eta^{\pm}$ which in [27] is defined as a function of the carrier injection components at threshold and transparency. The occupation probability of the ES at GS threshold for linear polarization can be obtained by applying the GS threshold condition $h_1(2f^{\pm}_{GS} - 1) = 1$ to the steady-state solution of (3):

$$f^{\pm}_{ES}|_{GS,th} = \frac{\gamma_n}{2\gamma_{21}}\frac{h_1 + 1}{h_1 - 1}. \quad (12)$$

Likewise, substituting expression (12) in (2) for the steady state yields the WL occupation probability at GS threshold:

$$f^{\pm}_{WL}|_{GS,th} = 4\frac{1}{\gamma_0}\frac{N_{QD}}{N_{WL}}\frac{2\gamma_{21}(h_1 - 1)}{2\gamma_{21}(h_1 - 1) - \gamma_n(h_1 + 1)}\left[\frac{\gamma_n}{2\gamma_{21}}\frac{h_1 + 1}{h_1 - 1}(\gamma_n + \gamma_{21}\frac{h_1 - 1}{2h_1})\right]. \quad (13)$$

The injection current at GS threshold is obtained from the steady-state solution of (1)

$$I^{\pm}|_{GS,th} = 4eAN_{QD}\left[1 + \frac{\gamma_n}{\gamma_0}\frac{2\gamma_{21}(h_1 - 1)}{2\gamma_{21}(h_1 - 1) - \gamma_n(h_1 + 1)}\right] \quad (14)$$

where

$$A = \frac{\gamma_n}{2\gamma_{21}}\frac{h_1 + 1}{h_1 - 1}\left(\gamma_n + \gamma_{21}\frac{h_1 - 1}{2h_1}\right) \quad (15)$$

In the expression of (14), there is no spin dependence, hence the superscript $\pm$ is dropped on the threshold pumping terms $I_{GS,th}$ from here on. The thresholds for

simultaneous ES and GS lasing are obtained by setting (4) and (5) equal to zero:

$$f_{GS}^{\pm}|_{th} = \frac{h_1+1}{2h_1} \tag{16}$$

$$f_{ES}^{\pm}|_{th} = \frac{h_2+1}{2h_2}. \tag{17}$$

Then, the steady-state solution of (2) by substituting (16) and (12) yields the occupation probability for the WL when both ES and GS lase:

$$f_{WL}^{\pm}|_{ES,th} = 4\frac{1}{\gamma_0}\frac{N_{QD}}{N_{WL}}\frac{2h_2}{h_2-1} \times\left[\frac{h_2+1}{2h_2}\left(\gamma_n+\gamma_{21}\frac{h_1-1}{2h_1}\right)\right]. \tag{18}$$

Finally, the steady-state solution of (1) gives the value of the injection current at the threshold of the excited state:

$$I^{\pm}|_{ES,th} = 4eBN_{QD}\left[1+\frac{\gamma_n}{\gamma_0}\frac{2h_2}{(h_2-1)}\right] \tag{19}$$

where

$$B = \frac{h_2+1}{2h_2}\left(\gamma_n+\gamma_{21}\frac{h_1-1}{2h_1}\right) \tag{20}$$

In the following, as for (14), we drop the superscript $\pm$ for the threshold pumping terms $I_{ES,th}$. Employing (6)–(11) along with (14) and (19) the normalized form of modified SFM REs (equations (1)–(5)) is:

$$\frac{dn_{WL}^{\pm}}{dt} = \frac{h_2}{e}[\eta^{\pm}(I_{ES,th}-I_{GS,th})+I_{GS,th}] -\gamma_0 n_{WL}^{\pm}\left(\frac{h_2-n_{ES}^{\pm}}{2h_2}\right)-\gamma_n n_{WL}^{\pm}\mp\gamma_s(n_{WL}^{+}-n_{WL}^{-}) \tag{21}$$

$$\frac{dn_{ES}^{\pm}}{dt} = \frac{1}{4}\left(\frac{h_2-n_{ES}^{\pm}}{h_2}\right)-\gamma_n(h_2+n_{ES}^{\pm})-\gamma_{21}(h_2+n_{ES}^{\pm}) \times\left(\frac{h_1-n_{GS}^{\pm}}{2h_1}\right)-2\gamma_n n_{ES}^{\pm}|E_{s,ES}^{\pm}|^2\mp\gamma_s(n_{ES}^{+}-n_{ES}^{-}) \tag{22}$$

$$\frac{dn_{GS}^{\pm}}{dt} = \gamma_{21}\left(\frac{h_2+n_{ES}^{\pm}}{h_2}\right)(h_1-n_{GS}^{\pm})-\gamma_n(h_1+n_{GS}^{\pm}) -2\gamma_n n_{GS}^{\pm}|E_{s,GS}^{\pm}|^2\mp\gamma_s(n_{GS}^{+}-n_{GS}^{-}) \tag{23}$$

$$\frac{dE_{s,GS}^{\pm}}{dt} = k(n_{GS}^{\pm}-1)(1+i\alpha)E_{s,GS}^{\pm} -(\gamma_a+i\gamma p)E_{s,GS}^{\pm} \tag{24}$$

$$\frac{dE_{s,ES}^{\pm}}{dt} = k(n_{ES}^{\pm}-1)(1+i\alpha)E_{s,ES}^{\pm} -(\gamma_a+i\gamma p)E_{s,ES}^{\pm}. \tag{25}$$

3 Results and discussion

The impact of the ES on the chaotic dynamics of QD spin-VCSELs is studied with the numerical solution of equations (21)–(25). The dynamics of the device is mapped into the P-η plane where P is the pump ellipticity,

$$P = \frac{\eta^{+}-\eta^{-}}{\eta^{+}+\eta-}$$

and η is the total pump intensity.

$$\eta = \eta^{+}+\eta^{-} \tag{26}$$

The pair P,η can control dynamically the stability of the emitted polarized fields [32–34] and it is commonly used for the investigation of the nonlinear dynamics of spin VCSELs. We identify and quantify chaotic nonlinearities by means of the LLE method. The LLE method has been applied previously for the analysis of injection locked lasers [31] and QD spin VCSELs accounting for WL and GS only [6]. A concise review of the theoretical treatment and numerical evaluation of the LLE can be found in [35]. Here, we summarize the main aspects of the method. The Lyapunov exponents are measures of the average rate of growth (or shrinking) of small perturbations to the solutions of a dynamical system. The value of the LLE is an indicator of the chaotic or regular nature of orbits in the phase space of the dynamical system, i.e., the time evolution of the solutions of the RE (21)–(25). In practice, the LLE is computed by following in time the evolution of two nearby orbits characterized by a small initial distance d_0 (of the order of 10^{-8}). After evolving the two orbits for one integration time step τ, the new distance d_1 between the evolved orbits is measured and the quantity $\ln\left(\frac{d_1}{d_0}\right)$ is calculated. This process is applied repeatedly and after N time steps the value of the LLE is estimated as

$$\mathrm{LLE} = \frac{1}{N\tau}\sum_{j=1}^{N}\ln\left(\frac{d_j}{d_{j-1}}\right) \tag{27}$$

(see [35] for more details on the practical computation of the LLE). Positive values of the LLE correspond to chaotic behavior, while negative values indicate stable solutions. Zero values of the LLE may be associated with periodic solutions and limit cycles. The LLE is considered as one of the most efficient ways to identify, and at the same time quantify, chaos for a dynamical system.

Given that the QD system under study can exhibit simultaneously two-state lasing, it is instructive to separate the trajectories for GS and ES transitions. The related LLEs are computed for the fields $E^{\pm}_{s,GS}$ and $E^{\pm}_{s,ES}$ by, respectively, considering the distances d_{GS} and d_{ES}:

$$d_1^{ES} = \begin{pmatrix} (n_a^{GS,+} - n_b^{GS,+})^2 + (n_a^{GS,-} - n_b^{GS,-})^2 + \\ (n_a^{ES,+} - n_b^{ES,+})^2 + (n_a^{ES,-} - n_b^{ES,-})^2 + \\ (n_a^{WL,+} - n_b^{WL,+})^2 + (n_a^{WL,-} - n_b^{WL,-})^2 \\ Re((E_a^{ES,+} - E_b^{ES,+}))^2 \\ +Im((E_a^{ES,+} - E_b^{ES,+}))^2 \\ +Re((E_a^{ES,-} - E_b^{ES,-}))^2 \\ +Im((E_a^{ES,-} - E_b^{ES,-}))^2 \end{pmatrix}^{1/2} \tag{28}$$

$$d_1^{GS} = \begin{pmatrix} (n_a^{GS,+} - n_b^{GS,+})^2 + (n_a^{GS,-} - n_b^{GS,-})^2 + \\ (n_a^{ES,+} - n_b^{ES,+})^2 + (n_a^{ES,-} - n_b^{ES,-})^2 + \\ (n_a^{WL,+} - n_b^{WL,+})^2 + (n_a^{WL,-} - n_b^{WL,-})^2 \\ \\ Re((E_a^{GS,+} - E_b^{GS,+}))^2 \\ +Im((E_a^{GS,+} - E_b^{GS,+}))^2 \\ +Re((E_a^{GS,-} - E_b^{GS,-}))^2 \\ +Im((E_a^{GS,-} - E_b^{GS,-}))^2 \end{pmatrix}^{1/2} . \tag{29}$$

Using Eqs. (27)–(29), the LLE can be calculated. Previous works on the use of LLE formalism in spin VCSELs (e.g., [31]) have overlooked the required integration time for numerically sound results. Although the trends and mapping are qualitatively correct, the quantitative claims (e.g., LLE values for chaos) are questionable. Recently, this was addressed in a tolerance analysis of the LLE against integration time [36]. Figure 2 shows the variation of LLE for the ES and GS with integration time. For the derivation of Fig. 2, we used the following parameters: for $\gamma_n = 1\,ns^{-1}$, $\gamma_0 = 400\,ns^{-1}$, $\gamma_s = 10ns^{-1}$, $\gamma_p = 20ns^{-1}$, α=3, h=1.1995, $k = 250ns^{-1}$, $P = 0.15128$ and η=2.276 . Throughout all the simulations in this contribution, the value of γ_a was set to zero to keep up with the approach followed in [37]. Based on this, we choose an integration time of 300ns for all subsequent simulations, which is a fair compromise between computational burden and accuracy. Regardless of the integration time, the values of the LLE for the ES and GS differ. We will elaborate on this in the subsequent analysis.

3.1 Effect of γ_{21}, γ_s and γ_p on chaotic dynamics

To study the effect of characteristic parameters of the device, namely the intra-dot relaxation rate γ_{21} the normalized gain coefficient h, the spin relaxation rate γ_s and the birefringence

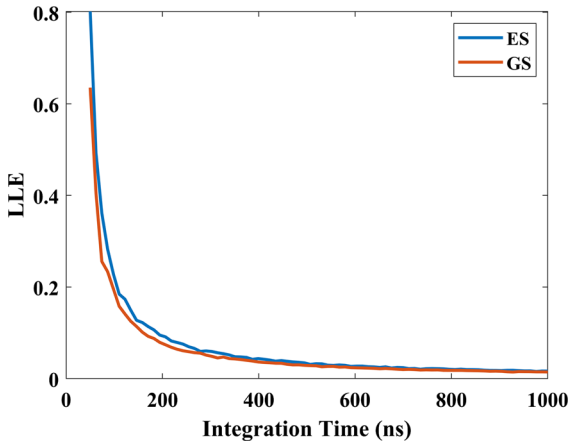

Fig. 2 LLE change with integration time for the time trace of Fig. 4a

rate γ_p on the dynamics of the output ES and GS intensities, stability maps in the P-η plane have been constructed. Figure 3 shows maps of P and η calculated for three different values of γ_{21} ($10\ ns^{-1}$, $50\ ns^{-1}$ and $150\ ns^{-1}$) for the following set of parameters: γ_n=$1\,ns^{-1}$, γ_0=$400ns^{-1}$, γ_s= $10ns^{-1}$, γ_p=$20ns^{-1}$, α=3, k=$250ns^{-1}$ and h_1=1.1995. These are in the range of previously reported values [38–40]. It is noted that works [26,40], on the α factor for QD lasers have challenged conventional practices of using the same value for both ES and GS emission. Additionally, the reported values for QD lasers vary from very small [19,41], to very large values [24,28]. For the α factor we choose the value of 3 for GS and 1.5 for ES, in accordance with previous works [6,27] in the middle of the range of the reported values for QD lasers.

The maps are quantified by means of LLE as described above. Schematically this is represented with different colors associated with the value of the LLE for a given pair of P-η as shown in the color bar at the top of the maps. The contour maps are symmetric around $P = 0$, therefore negative values of P are omitted. For the case of relatively low ES–GS coupling strength (γ_{21}=$10\ ns^{-1}$) in Fig. 3a and b there exists an extended unstable region ($LLE > 0$) for a broad range of total pump intensity η. The dynamic behavior of GS and ES emission exhibit the same kind of dynamics (chaotic behavior or stability) throughout the P-η plane. This is expected since both transitions are fed from the same reservoir of carriers.

However, it is noticeable that the amount of nonlinearity is not identical, in other words the value of LLE for the two cases is not the exact same. This is evident in Fig. 3a and b, where the values of LLE for ES and GS emission agree on the sign but differ on the actual value that is, in the amount of chaos. This justifies our choice of the LLE method over other methods commonly used for the study of nonlinearities, e.g., bifurcation theory, as LLE can identify and at the same time quantify chaos. Figure 4a shows the time series for the point (P,η)=(0.15128, 2.276) of Fig. 3a and b for which $LLE > 0$

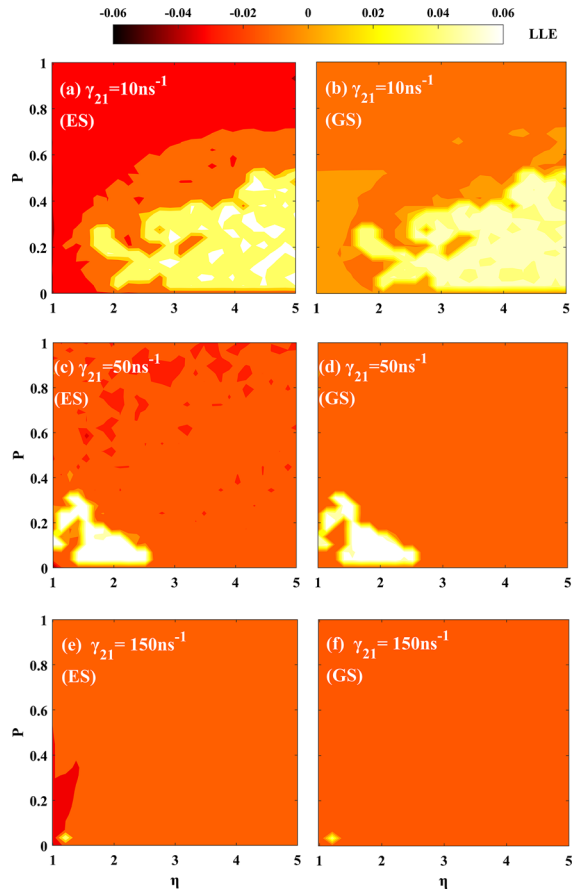

Fig. 3 Calculated maps of LLE values in the P-η plane for two-state QD spin-VCSEL for 3 different values of γ_{21}=[$10ns^{-1}$, $50ns^{-1}$, $150ns^{-1}$] for ES (**a**), (**c**), (**e**), and for GS (**b**), (**d**), (**f**). The color bar at the top corresponds to the LLE values

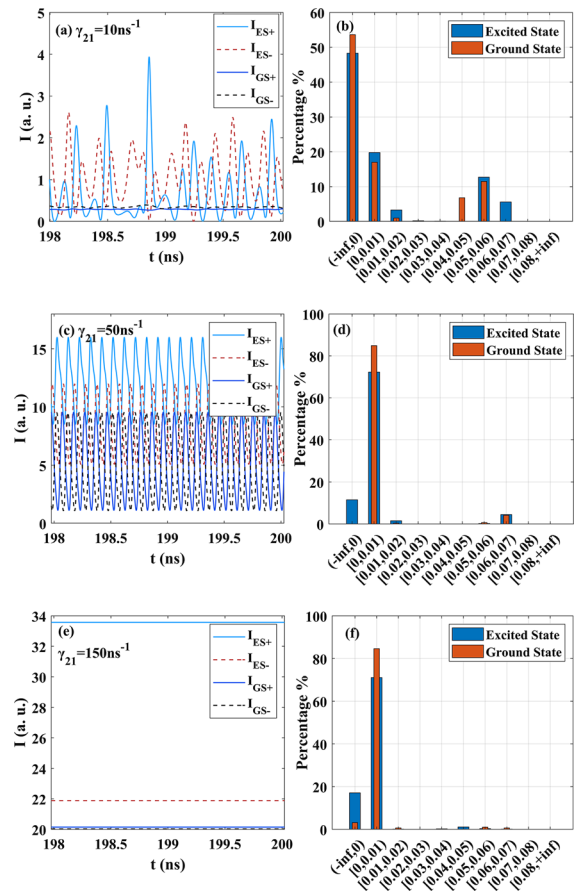

Fig. 4 **a**, **c**, **e**) Time series for the point $(P, \eta) = (0.15128, 2.276)$ for γ_n=$1ns^{-1}$, γ_0=$400ns^{-1}$, γ_s=$10ns^{-1}$, γ_p=$20ns^{-1}$, $\alpha = 3$, $h = 1.1995$, k = $250ns^{-1}$, $P = 0.15128$ and $\eta = 2.276$. b, d, f) Percentage of points of the maps in Fig. 3 having LLE in particular value intervals

for both GS and ES emissions for clockwise and anticlockwise circular polarization. The difference between ES and GS emission in terms of amplitude is emphatic. This is expected as for dual emission QD lasers, when ES mode reaches its lasing threshold the GS mode saturates [31]. Although, both GS and ES emission exhibit chaotic behavior with similar (not identical) LLE values, their time evolution differs. This asymmetry in the dynamics of the GS and ES related emission is illustrated in Fig. 4b where the bar charts depict the percentage of points of the stability maps for ES and GS emission that lie within specific LLE intervals. It is interesting to note that while both ES and GS exhibit similar chaotic behavior, the amplitude of the GS is suppressed compared to ES when the injected spin-polarized carriers in the quantum dot are captured in the ES (and eventually recombined with holes in the Valence Band (VB)) much faster than they decay in the GS level. As a result, the lasing occurs primarily from the ES leading the GS intensity suppression.

In Fig. 3c–f, we explore further the effect of intraband relaxation rate of ES to GS, for γ_{21}=$50ns^{-1}$ and γ_{21}=$150ns^{-1}$. Unlike Fig. 3a and b, the chaotic regions in the P-η plane are now shrunk, in other words chaotic behavior can be quenched by means of γ_{21}. This is evident in Fig. 4c and e, where the time series for the same (P,η)=(0.15128, 2.276) as in Fig. 4a, are plotted along with the distribution of LLE (Fig. 4d and f). In Fig. 4c, e, both ES and GS emission is constant (periodic) in time (LLE value close to zero) as a result of the suppression of the chaotic dynamics induced by the increase in the intra-dot relaxation rate.

The effect of the birefringence rate γ_p and the spin relaxation rate γ_s is well established on the type of dynamics (chaos, periodicity or stability) [42]. γ_p and γ_s can be used to tune the asymmetry in the details, not the type, of the dynamics of ES and GS. In Fig. 5, we map the dynamics in the plane of γ_p and γ_s for the point (P,η)=(0.0513,2.2410) for the ES (Fig. 5a) and GS (Fig. 5b). This point in Fig.3a and b is associated to a

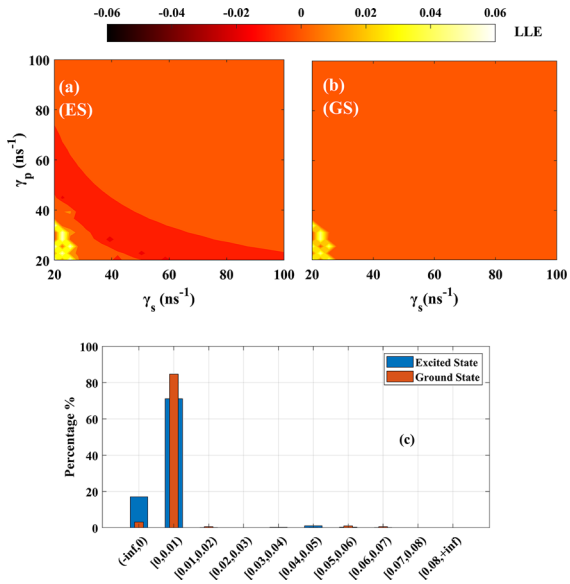

Fig. 5 **a** ES γ_s-γ_p LLE value maps for two-state QD spin-VCSEL, **b** GS γ_s-γ_p maps for two-state QD spin-VCSEL for γ_n=1 ns^{-1}, γ_0=400 ns^{-1}, γ_s=10 ns^{-1}, γ_p=20 ns^{-1}, α=3, k=250ns^{-1}, h=1.1995, γ_{21}=10ns^{-1}, P=0.0513 and η=2.241). **c** Percentage of points of the maps in Fig. 5a and b having LLE in particular value intervals

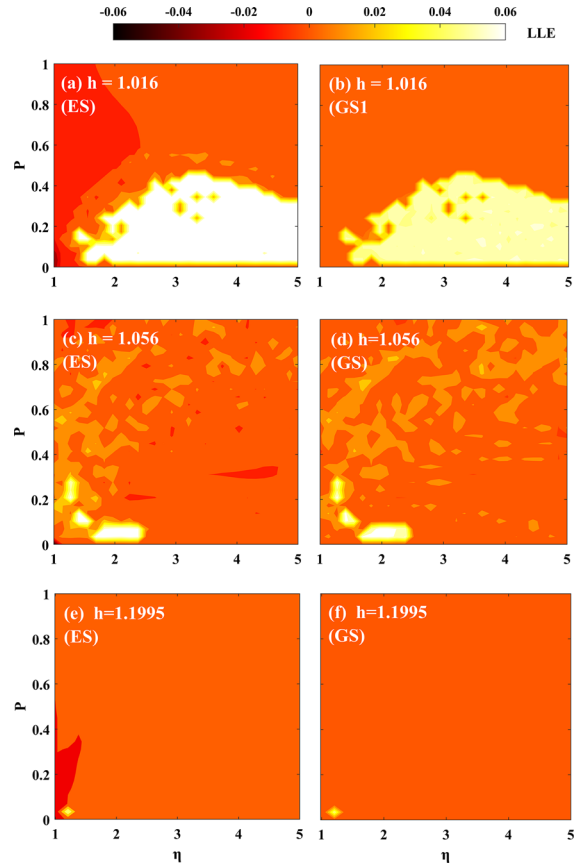

Fig. 6 Calculated maps of LLE values in the $P - \eta$ plane for two-state QD spin-VCSEL for ES (**a**, **c**, **e**) and for GS (**b**, **d**, **f**) for $h = 1.019$ (a, b), $h = 1.016$ (c, d) and $h = 1.1995$ (e, f) for the set of parameters $\gamma_n = 1\,ns^{-1}$, $\gamma_0 = 400\,ns^{-1}$, $\gamma_s = 10\,ns^{-1}$, $\gamma_p = 20\,ns^{-1}$, $\gamma_{21} = 150\,ns^{-1}$, $\alpha = 3$, and $k = 250\,ns^{-1}$. The color bar at the top corresponds to the LLE values

positive largest Lyapunov exponent. Thus, a point of irregular dynamical behavior. The purpose of Fig. 5 is to illustrate the impact of the variation of γ_s and γ_p rates to the dynamics of QD spin-VCSELs. Therefore, we decided to choose a random point in the P-η plane from Fig. 3a and b (preferably a point with irregular behavior) to examine if the asymmetry of LLE values between ES and GS, observed previously in the P-η plane (Fig. 3a–f), is preserved under the variation of a different set of bifurcation parameters. The rest of parameters are γ_n=1ns^{-1}, γ_0=400ns^{-1}, α=3, k=250ns^{-1}, and h=1.1995. For this (P,η) point and the particular set of parameters, the spin-polarized QD-VCSEL exhibits stable behavior. Variation of γ_p and γ_s exert nonlinear effects that span the full range of dynamics from stability to chaos for both ES and GS. Figure 5c quantifies the effect of γ_p and γ_s on the magnitude of chaos in the ES and GS dynamics. Again, in this case (as in the previous, where the value of γ_{21} varied) the amount of chaos experienced by ES and GS differs quantitatively.

3.2 Effect of h on chaotic dynamics

The effect on the chaotic dynamics of a QD spin-VCSEL under the variation the normalized gain coefficient is depicted in Fig. 6. Again, as in Fig. 3, the dynamics are mapped in the P-η plane. Fig. 6a, c and e is for ES and Fig. 6b, d and f is for GS. Initially, for a small value of h, ($h = 1.016$) a broad region of complex dynamics is observed for both ES and GS in Fig. 6a and b. Although the qualitative dynamical characteristics of ES and GS are identical, quantitative differences occur as the LLE value denotes. By increasing the value of h, from h=1.056 (Fig. 6c and d) to h=1.1995 (Fig. 6e and f) these regions of chaotic behavior are shrunk dramatically. Again, the dynamical qualitative symmetry is observed as well as the quantitative asymmetry between ES and GS. The variation of h, has a similar (if not identical) trend as γ_{21} (Fig. 3) in the dynamics of the device.

The quantitative difference between the chaotic ES and GS dynamics can be verified also by means of the Correlation Coefficient (CC) [43]. Figure 7a and b shows the LLE values of the point $P = 0.1724$ and η=1.9660 in the plane γ_{21}-h. For small values of h the LLE value is positive, indicating complex (chaotic) behavior for all values of γ_{21}. As γ_{21} increases the device is more stable. Although the dynamics are identical for ES and GS the dynamical quantitatively asymmetry occurs once again, as in the previous cases.

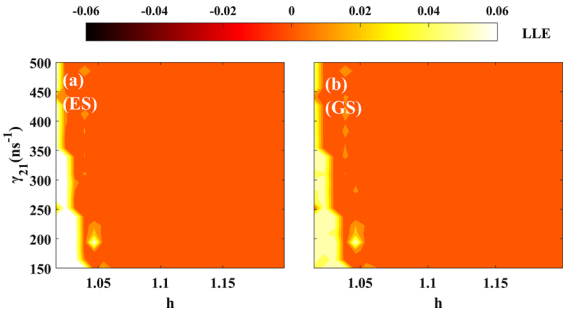

Fig. 7 Calculated LLE maps in the γ_{21} - h plane for two-state QD spin-VCSEL for **a** ES and **b** GS for the set of parameters $\gamma_n = 1\,ns^{-1}$, $\gamma_0 = 400\,ns^{-1}$, $\gamma_s = 10\,ns^{-1}$, $\gamma_p = 20\,ns^{-1}$, $\alpha = 3$, $k = 250\,ns^{-1}$, $P = 0.1724$, and $\eta = 1.9660$

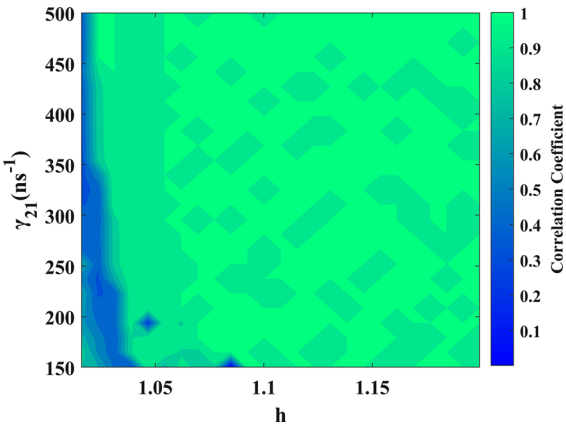

Fig. 8 Calculated CC value map in the plane $\gamma_{21} - h$ for the set of parameters $\gamma_n = 1\,ns^{-1}$, $\gamma_0 = 400\,ns^{-1}$, $\gamma_s = 10\,ns^{-1}$, $\gamma_p = 20\,ns^{-1}$, $\alpha = 3$, k $= 250\,ns^{-1}$, $P = 0.1724$, and $\eta = 1.9660$

This behavior, previously decoded by the LLE, is validated in Fig. 8 where the values of CC are depicted. It is worth noting that the topographical characteristics of Fig. 7a and b and Fig. 8 are identical. The small values of CC found in the chaotic regions indicate that ES and GS are uncorrelated to each other. In regions of stable operation the CC has values close to the unity implying that both ES and GS are correlated.

4 QD spin-VCSELs as a platform for reservoir computing

The uncorrelated dynamics of the ES and GS emission of the spin QD-VCSELs studied here can be beneficial for Reservoir Computing (RC).

RC is a brain-inspired computational paradigm that can address computationally demanding tasks (see for example [44] the references therein) including speech recognition [45] and chaotic systems prediction [46]. More relevant to the scopes of the present study are the RC realizations based on VCSELs; exploiting the polarization dynamics of conventional VCSELs, Vatin and co-workers [47] demonstrated superior RC performance compared to single mode laser based RC systems. The concept of VCSEL based RC was elaborated by Guo et al. [48] who used mutually coupled VCSELs for RC that offer fourfold improvements in information processing rate.

In terms of performance, a photonic RC system is more efficient when operated 'at the edge of chaos' [49,50] in other words for small LLE values [51]. The LLE formalism is particularly suited in identifying the areas of weak chaos as depicted in the stability maps produced here. Additionally, Bogris et al. [52] showed for a RC system based on a multi-mode Fabry–Perot laser that the performance is optimized when the modes are weakly correlated. Our proposed structure is a platform for tailoring both the amount of chaos and correlation of the output polarization of the lasing modes (ES and GS) and as such it is expected that it will prove ideal for reservoir computers.

5 Conclusions

We investigated the impact of the ES lasing on the chaotic dynamics of a QD spin-VCSELs. We extended the modified SFM used previously for the study of GS only QD spin VCSEL to account for ES. The dynamics were studied by means of the LLE as it is most suited for quantification of nonlinearities. The maps of the dynamics in the plane of the control parameters P (pump ellipticity) and η (pump amplitude), exhibit large areas of instabilities for relatively low values of ES to GS intra-band, γ_{21}, rates which shrink for larger values of γ_{21}. A similar behavior is observed when the normalized gain coefficient, h, increases from low values to larger ones. Interestingly, the dynamics of the ES and GS emissions, although of the same type throughout the computed LLE maps, differ in the amount of the nonlinearity and this difference can be tuned with proper choice of γ_p and γ_s. The asymmetry in the ES and GS emission dynamics was verified using the CC. It is anticipated that the latter findings will be of high interest for RC applications.

Acknowledgements The authors acknowledge helpful discussions with Prof. Mike Adams of the School of Computer Science and Electronic Engineering, University of Essex, UK.
P. Georgiou and G. Mourkioti acknowledge financial support from University of Patras, Basic Research Program 'K Karatheodori' (56890000).

Declarations

Conflict of interest The authors declare that they have no conflict of interest.

Data availability The datasets generated during the current study are available from the corresponding author on reasonable request.

References

1. Lindemann, M., Jung, N., Stadler, P., Pusch, T., Michalzik, R., Hofmann, M., Gerhardt, N.C.: Bias current and temperature dependence of polarization dynamics in spin-lasers with electrically tunable birefringence. AIP Adv. **10**(3), 035211 (2020)
2. Yokota, N., Ikeda, K., Yasaka, H.: Numerical investigation of direct IQ modulation of spin-VCSELs for coherent communications. Spintron. XIII **11470**, 114702I (2020)
3. Song, T., Xie, Y., Ye, Y., Liu, B., Chai, J., Jiang, X., Zheng, Y.: Numerical analysis of nonlinear dynamics based on spin-VCSELs with optical feedback. Photonics **8**, 10 (2021)
4. Lindemann, M., Jung, N., Burghard, M., Pusch, T., Xu, G., Žutić, I., Birkedal, D., Michalzik, R., Hofmann, M.R., Gerhardt, N.C.: Intensity and polarization dynamics in ultrafast birefringent spin-VCSELs. Spintronics XIII **11470**, 114702H (2020)
5. Li, N., Susanto, H., Cemlyn, B., Henning, I., Adams, M.: Secure communication systems based on chaos in optically pumped spin-VCSELs. Opt. Lett. **42**(17), 3494–3497 (2017)
6. Adams, M.J., Alexandropoulos, D.: Analysis of quantum-dot spin-VCSELs. IEEE Photonics J. **4**(4), 1124–1132 (2012)
7. Lee, J., Oszwałdowski, R., Gøthgen, C., Žutić, I.: Mapping between quantum dot and quantum well lasers: from conventional to spin lasers. Phys. Rev. B **85**(4), 045314 (2012)
8. Li, N., Alexandropoulos, D., Susanto, H., Henning, I., Adams, M.: Stability analysis of quantum-dot spin-VCSELs. Electronics **5**(4), 83 (2016)
9. Torre, M.S., Susanto, H., Li, N., Schires, K., Salvide, M., Henning, I., Adams, M., Hurtado, A.: High frequency continuous birefringence-induced oscillations in spin-polarized vertical-cavity surface-emitting lasers. Opt. Lett. **42**(8), 1628–1631 (2017)
10. Lindemann, M., Xu, G., Pusch, T., Michalzik, R., Hofmann, M.R., Žutić, I., Gerhardt, N.C.: Ultrafast spin-lasers. Nature **568**(7751), 212–215 (2019)
11. Prucnal, P.R., Shastri, B.J.: Neuromorphic Photonics. CRC Press, Boca Raton (2017)
12. Zhang, Z., Wu, Z., Lu, D., Xia, G., Deng, T.: Controllable spiking dynamics in cascaded VCSEL-SA photonic neurons. Nonlinear Dyn. **99**(2), 1103–1114 (2020)
13. Deng, T., Xia, G., Wu, Z.: Broadband chaos synchronization and communication based on mutually coupled VCSELs subject to a bandwidth-enhanced chaotic signal injection. Nonlinear Dyn. **76**(1), 399–407 (2014)
14. Holub, M., Bhattacharya, P.: Spin-polarized light-emitting diodes and lasers. J. Phys. D Appl. Phys. **40**(11), R179 (2007)
15. Alharthi, S., Orchard, J., Clarke, E., Henning, I., Adams, M.: 1300 nm optically pumped quantum dot spin vertical external-cavity surface-emitting laser. Appl. Phys. Lett. **107**(15), 151109 (2015)
16. Schires, K., Hurtado, A., Henning, I.D., Adams, M.J.: Polarization and time-resolved dynamics of a 1550-nm vcsel subject to orthogonally polarized optical injection. IEEE Photonics J. **3**(3), 555–563 (2011)
17. Alharthi, S., Hurtado, A., Al Seyab, R.K., Korpijarvi, V.M., Guina, M., Henning, I., Adams, M.: Control of emitted light polarization in a 1310 nm dilute nitride spin-vertical cavity surface emitting laser subject to circularly polarized optical injection. Appl. Phys. Lett. **105**(18), 181106 (2014)
18. Gahl, A., Balle, S., Miguel, M.S.: Polarization dynamics of optically pumped VCSELs. IEEE J. Quantum Electron. **35**(3), 342–351 (1999)
19. Li, N., Susanto, H., Cemlyn, B., Henning, I., Adams, M.: Mapping bifurcation structure and parameter dependence in quantum dot spin-VCSELs. Opt. Express **26**(11), 14636–14649 (2018)
20. Mu, P., Pan, W., Li, N.: Analysis and characterization of chaos generated by free-running and optically injected VCSELs. Opt. express **26**(12), 15642–15655 (2018)
21. Drong, M., Fördös, T., Jaffrès, H., Postava, K., Peřina, J., Jr., Drouhin, H.J., Pištora, J.: Dynamical and anisotropic properties of spin-VCSELs. Quantum Sens. Nano Electron. Photonics **10926**, 1092614 (2019)
22. Žutić, I., Xu, G., Lindemann, M., Junior, P.E.F., Lee, J., Labinac, V., Stojšić, K., Sipahi, G.M., Hofmann, M.R., Gerhardt, N.C.: Spin-lasers: spintronics beyond magnetoresistance. Solid State Commun. **316**, 113949 (2020)
23. Drong, M., Fördös, T., Jaffrès, H., Peřina, J., Jr., Postava, K., Ciompa, P., Pištora, J., Drouhin, H.J.: Spin-vcsels with local optical anisotropies: toward terahertz polarization modulation. Phys. Rev. Appl. **15**(1), 014041 (2021)
24. Bhattacharya, P., Basu, D., Das, A., Saha, D.: Quantum dot polarized light sources. Semicond. Sci. Tech. **26**(1), 014002 (2010)
25. Xiao, J.L., Guo, C.C., Ji, H.M., Xu, P.F., Yao, Q.F., Lv, X.M., Zou, L.X., Long, H., Yang, T., Huang, Y.Z.: Measurement of linewidth enhancement factor for 1.3-*mu*m InAs/GaAs quantum dot lasers. IEEE Photonics Tech. Lett. **25**(5), 488–491 (2013)
26. Dagens, B., Markus, A., Chen, J., Provost, J.G., Make, D., Le Gouezigou, O., Landreau, J., Fiore, A., Thedrez, B.: Giant linewidth enhancement factor and purely frequency modulated emission from quantum dot laser. Electron. Lett. **41**(6), 323–324 (2005)
27. Alexandropoulos, D., Al-Seyab, R., Henning, I., Adams, M.: Instabilities in quantum-dot spin-VCSELs. Opt. Lett. **37**(10), 1700–1702 (2012)
28. Oszwałdowski, R., Gøthgen, C., Žutić, I.: Theory of quantum dot spin lasers. Physical Review B **82**(8), 085,316 (2010)
29. Qasaimeh, O.: Novel closed-form solution for spin-polarization in quantum dot VCSEL. Opt. Commun. **350**, 83–89 (2015)
30. Olejniczak, L., Panajotov, K., Wieczorek, S., Thienpont, H., Sciamanna, M.: Intrinsic gain switching in optically injected quantum dot laser lasing simultaneously from the ground and excited state. JOSA B **27**(11), 2416–2423 (2010)
31. Chlouverakis, K.E., Adams, M.J.: Stability maps of injection-locked laser diodes using the largest Lyapunov exponent. Opt. Commun. **216**(4–6), 405–412 (2003)
32. Schires, K., Al Seyab, R., Hurtado, A., Korpijarvi, V.M., Guina, M., Henning, I.D., Adams, M.J.: Optically-pumped dilute nitride spin-VCSEL. Opt. Express **20**(4), 3550–3555 (2012)
33. Schires, K., Al Seyab, R., Hurtado, A., Korpijärvi, V.M., Guina, M., Henning, I.D., Adams, M.J.: Instabilities in optically-pumped 1300nm dilute nitride spin-VCSELs: experiment and theory. In: IEEE Photonics Conference 2012, pp. 870–871. IEEE (2012)

34. Alharthi, S.S., Al Seyab, R.K., Henning, I.D., Adams, M.J.: Simulated dynamics of optically pumped dilute nitride 1300 nm spin vertical-cavity surface-emitting lasers. IET Optoelectron. **8**(2), 117–121 (2014)
35. Skokos, C.: The Lyapunov characteristic exponents and their computation. In: Souchay, J., Dvorak, R. (eds.) Dynamics of Small Solar System Bodies and Exoplanets. Lecture Notes in Physics, vol. 790. Springer, Berlin, Heidelberg (2010). https://doi.org/10.1007/978-3-642-04458-8_2
36. Georgiou, P.D., Alexandropoulos, D., Skokos, C.: Study of the dynamics of spin-polarized vertical cavity surface emitting lasers using largest Lyapunov Exponent. In: 2020 22nd International Conference on Transparent Optical Networks (ICTON), pp. 1–3. IEEE (2020)
37. Adams, M.J., Alexandropoulos, D.: Parametric analysis of spin-polarized VCSELs. IEEE J. Quantum Electron. **45**(6), 744–749 (2009)
38. Nizette, M., Sciamanna, M., Gatare, I., Thienpont, H., Panajotov, K.: Dynamics of vertical-cavity surface-emitting lasers with optical injection: a two-mode model approach. JOSA B **26**(8), 1603–1613 (2009)
39. Markus, A., Chen, J., Paranthoen, C., Fiore, A., Platz, C., Gauthier-Lafaye, O.: Simultaneous two-state lasing in quantum-dot lasers. Appl. Phys. Lett. **82**(12), 1818–1820 (2003)
40. Lingnau, B., Chow, W.W., Schöll, E., Lüdge, K.: Feedback and injection locking instabilities in quantum-dot lasers: a microscopically based bifurcation analysis. New J. Phys. **15**(9), 093031 (2013)
41. Gerhardt, N.C., Hofmann, M.R.: Spin-controlled vertical-cavity surface-emitting lasers. Adv. Opt. Tech. **2012**,(2012)
42. Zubov, F., Maximov, M., Moiseev, E., Savelyev, A., Shernyakov, Y., Livshits, D., Kryzhanovskaya, N., Zhukov, A.: Observation of zero linewidth enhancement factor at excited state band in quantum dot laser. Electron. Lett. **51**(21), 1686–1688 (2015)
43. Virte, M., Sciamanna, M., Panajotov, K.: Synchronization of polarization chaos from a free-running VCSEL. Opt. Lett. **41**(19), 4492–4495 (2016)
44. Paquot, Y., Duport, F., Smerieri, A., Dambre, J., Schrauwen, B., Haelterman, M., Massar, S.: Optoelectronic reservoir computing. Sci. Rep. **2**(1), 1–6 (2012)
45. Verstraeten, D., Schrauwen, B., Stroobandt, D.: Reservoir-based techniques for speech recognition. In: The 2006 IEEE International Joint Conference on Neural Network Proceedings, pp. 1050–1053. IEEE (2006)
46. Pathak, J., Hunt, B., Girvan, M., Lu, Z., Ott, E.: Model-free prediction of large spatiotemporally chaotic systems from data: a reservoir computing approach. Phys. Rev. Lett. **120**(2), 024102 (2018)
47. Vatin, J., Rontani, D., Sciamanna, M.: Enhanced performance of a reservoir computer using polarization dynamics in VCSELs. Opt. Lett. **43**(18), 4497–4500 (2018)
48. Guo, X.X., Xiang, S.Y., Zhang, Y.H., Lin, L., Wen, A.J., Hao, Y.: Four-channels reservoir computing based on polarization dynamics in mutually coupled VCSELs system. Opt. Express **27**(16), 23293–23306 (2019)
49. Bertschinger, N., Natschläger, T.: Real-time computation at the edge of chaos in recurrent neural networks. Neural Comput. **16**(7), 1413–1436 (2004)
50. Cai, Q., Guo, Y., Li, P., Bogris, A., Shore, K.A., Zhang, Y., Wang, Y.: Modulation format identification in fiber communications using single dynamical node-based photonic reservoir computing. Photonics Res. **9**(1), B1–B8 (2021)
51. Sprott, J.: Chaotic dynamics on large networks. Chaos Interdiscip. J. Nonlinear Sci. **18**(2), 023135 (2008)
52. Bogris, A., Mesaritakis, C., Deligiannidis, S., Li, P.: Fabry-Perot lasers as enablers for parallel reservoir computing. IEEE J. Sel. Topics Quantum Electron. **27**(2), 1–7 (2020)